Thin films of a three-dimensional topological insulator in a strong magnetic field: Microscopic study

A. Pertsova,[1] C. M. Canali,[1] and A. H. MacDonald[2]
[1]*Department of Physics and Electrical Engineering, Linnæus University, 391 82 Kalmar, Sweden*
[2]*Department of Physics, University of Texas at Austin, Austin, Texas 78712, USA*
(Received 4 November 2014; revised manuscript received 10 February 2015; published 26 February 2015)

The response of thin films of Bi_2Se_3 to a strong perpendicular magnetic field is investigated by performing magnetic band-structure calculations for a realistic multiband tight-binding model. Several crucial features of Landau quantization in a realistic three-dimensional topological insulator are revealed. The $n = 0$ Landau level is absent in ultrathin films, in agreement with experiment. In films with a crossover thickness of five quintuple layers, there is a signature of the $n = 0$ level, whose overall trend as a function of magnetic field matches the established low-energy effective-model result. Importantly, we find a field-dependent splitting and a strong spin polarization of the $n = 0$ level, which can be measured experimentally at reasonable field strengths. Our calculations reveal mixing between the surface and bulk Landau levels, which causes the character of the levels to evolve with magnetic field.

DOI: 10.1103/PhysRevB.91.075430 PACS number(s): 73.20.−r, 71.70.Di

I. INTRODUCTION

The peculiar structure of the Landau levels (LLs) present in three-dimensional (3D) topological insulators (TIs) [1–3] in a strong magnetic field is a characteristic signature of their Dirac surface states [4–6]. In the simplest low-energy effective models, a field-independent $n = 0$ level emerges at the surface-state band-crossing energy that is analogous to the $n = 0$ level of another Dirac material, namely graphene [7], suggesting strong similarities in the magnetic-field response of these two systems. However, a number of important features have been observed recently in thin films of binary-chalcogenide 3D TIs, which indicate that the conventional picture of Landau quantization may not be fully applicable to these materials. The most notable features include (i) deviations from the square-root dependence of LL energies on the magnetic field and the LL index, which applies when linear dispersion is present over a wide energy regime [4], (ii) asymmetry of the LL spectrum with respect to the Dirac point [4,5], and (iii) finite-thickness effects, in particular the predicted splitting of the $n = 0$ level due to intersurface coupling [8–10] and its absence in ultrathin films [11]. LL positions are readily measured in scanning probe studies and, since they depend on both the zero-field energy bands and the momentum dependence of zero-field wave functions, they are a sensitive probe of the electronic structure.

In this work, we study the electronic properties of thin films of Bi_2Se_3 in the presence of a strong quantizing magnetic field, using a microscopic approach that captures the complex electronic structure and the intersurface hybridization of the realistic material. We perform magnetic band-structure calculations [12–14] using a multiband tight-binding (TB) model for Bi_2Se_3 [15,16]. We consider slabs of one to six quintuple layers (QLs) in magnetic fields of the order of 10 T (for the smallest thickness) and larger. We find that the $n = 0$ LL is absent in slabs with thicknesses below five QLs, but it starts to emerge at this crossover thickness, in agreement with experiments on a similar system (Sb_2Te_3) [11]. Importantly, the energy gap due to intersurface coupling, which is found at the Dirac point of 3D TI thin films at zero field [17], persists at finite magnetic fields.

This finding is partly consistent with recent theoretical studies, which investigated the effect of finite thickness on the LL spectrum either by introducing an *ad hoc* hybridization gap into the Dirac Hamiltonian of the surface states [9,10], or by using a minimal TB model [8] for a single-Dirac-cone family of 3D TIs. However, there are crucial differences between the results obtained with our microscopic approach and those obtained with effective models. The hybridization gap at finite magnetic fields emerges naturally in our electronic structure calculations for finite slabs. As a result, the degeneracy of the $n = 0$ level is lifted. For moderate field strengths, the gap increases approximately linearly with the field, with the dependence becoming weak with increasing thickness.

For five QLs, the field dependence of one of the two components of the $n = 0$ LL is in good agreement with the analytical expression derived by Liu *et al.* [18] using a four-band effective Hamiltonian [19]. The other component, which is energetically closer to the valence band, deviates further from the analytical curve for increasing magnetic fields, with its wave function becoming progressively bulklike. In the limit of small fields, the splitting approaches the value of the zero-field hybridization gap. The LLs of the bulk and surface states, which cannot be easily disentangled experimentally, are identified based on the spatial character of their wave functions. The splitting of the $n = 0$ LL can be detected by scanning tunneling spectroscopy (STS) experiments, and it can be used as a probe of pertinent electronic structure features.

The paper is organized as follows. In Sec. II, we describe the TB model and discuss the details of magnetic band-structure calculations. The numerical results, namely the calculated LL spectra and the analysis of the hybridization gap in the presence of an applied magnetic field for one to six QLs of Bi_2Se_3, are presented in Sec. III. We also briefly outline possible implications of our findings for measurable electronic properties of 3D TI thin films in magnetic field. Finally, we draw some conclusions.

II. MODEL

The electronic structure of a Bi_2Se_3 slab is described by an sp^3 TB model with parameters obtained by fitting to density

 ©2015 American Physical Society

functional theory (DFT) band structures [15,16]. The applied magnetic field is introduced via the Peierls substitution [20,21]. The Hamiltonian of the system reads

$$\hat{H}(\mathbf{k}) = \sum_{\substack{ii',\sigma \\ \alpha\alpha'}} \gamma_{ii'}^{\alpha\alpha'} e^{i\mathbf{k}\cdot\mathbf{r}_{ii'}} e^{-\frac{ie}{\hbar c}\int_i^{i'}\mathbf{A}\cdot d\mathbf{l}} \hat{c}_{i\alpha}^{\sigma\dagger}\hat{c}_{i'\alpha'}^{\sigma} + \sum_{\substack{i,\sigma\sigma' \\ \alpha\alpha'}} \lambda_i \langle i,\alpha,\sigma|\hat{\vec{l}}\cdot\hat{\vec{s}}|i,\alpha',\sigma'\rangle \hat{c}_{i\alpha}^{\sigma\dagger}\hat{c}_{i\alpha'}^{\sigma'}, \quad (1)$$

where $\mathbf{k}$ is the reciprocal-lattice vector, $i(i')$ is the atomic index, $\alpha(\alpha')$ labels atomic orbitals, and $\sigma(\sigma')$ denotes the spin. Here i runs over all atoms in the magnetic unit cell (see the definition below), while $i' \neq i$ runs over all neighbors of atom i, including atoms in the adjacent cells; $\mathbf{r}_{ii'}$ is the distance between atoms i and i' ($\mathbf{r}_{ii'} = 0$ for $i = i'$). $\gamma_{ii'}^{\alpha\alpha'}$ are the Slater-Koster parameters and $\hat{c}_{i\alpha}^{\sigma\dagger}$ ($\hat{c}_{i\alpha}^{\sigma}$) is the creation (annihilation) operator for an electron with spin σ at the atomic orbital α of site i. We include the hopping between nearest neighbors in the x-y plane and next-nearest neighbors along the z direction. The second term in Eq. (1) is the intra-atomic spin-orbit interaction, where $|i,\alpha,\sigma\rangle$ are spin- and orbital-resolved atomic orbitals, $\hat{\vec{l}}$ is the orbital angular momentum operator, and $\hat{\vec{s}}$ is the spin operator; λ_i is the SO strength.

The factors $e^{i\theta_{ii'}}$, with $\theta_{ii'} = -\frac{e}{\hbar c}\int_i^{i'}\mathbf{A}\cdot d\mathbf{l}$ ($\theta_{ii} = 0$), which multiply the hopping matrix elements in Eq. (1), are the Peierls phase factors. $\mathbf{A}$ is the magnetic vector potential and $\mathbf{l}$ is a straight path connecting the lattice sites i and i'. A uniform magnetic field is applied perpendicular to the surface of the slab, $\mathbf{B} = B\hat{z}$, and we use the Landau gauge, $\mathbf{A} = (0, B\hat{x}, 0)$. We focus on the orbital contribution of the magnetic field, which is expected to be the most crucial one for Landau quantization, at least for magnetic fields in the experimental range. Therefore, we do not consider the Zeeman term. We are concerned with the effect of the hybridization between the opposite surfaces, and between the surfaces and the valence band bulk, on the LL spectrum of Bi_2Se_3 thin films.

It is known that for electrons, subject to both magnetic field and a periodic potential, the electron wave function cannot satisfy the periodic boundary conditions [the Hamiltonian in Eq. (1) does not commute with the operator of translations]. However, one can introduce the new primitive translation vectors, which define the *magnetic unit cell*, provided that the magnetic flux ϕ threading a crystal unit cell is a rational multiple of the magnetic flux quantum $\phi_0 = hc/e$, i.e., $\phi = p\phi_0/q$, where p and q are mutually prime integers [12]. The magnetic unit cell, carrying a magnetic flux $p\phi_0$, is q times larger than the crystal unit cell (see Fig. 1). The corresponding magnetic Brillouin zone is q times smaller than the original one. This magnetic periodic boundary condition (MPBC) requirement guarantees that the electron wave function only accumulates a phase $2\pi p$ when one moves along the edges of the magnetic unit cell. It follows from the MPBC that the value of the magnetic field is determined by the size of the magnetic unit cell, i.e., $B = p\,\phi_0/S_m = p\,\phi_0/q\,S_0$, where S_m (S_0) is the area of the magnetic (crystal) unit cell in the plane perpendicular to the field. This is a notorious numerical limitation of magnetic band-structure calculations.

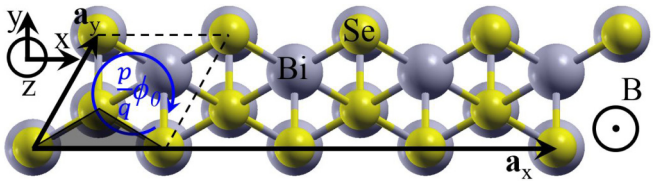

FIG. 1. (Color online) Top view (x-y plane) of the magnetic unit cell ($q = 4$) of five QLs of Bi_2Se_3. $\mathbf{a}_{x(y)}$ are the 2D lattice vectors. The magnetic field is along the z axis. The dashed lines show the crystal unit cell. The shaded triangle marks the elementary 2D placket.

The magnetic unit cell of a Bi_2Se_3 slab is built by replicating the slab unit cell q times along the x axis (Fig. 1). Its size grows as $q \times (5N_{QL})$, where N_{QL} is the number of QLs. With this constraint, we were able to reach minimum field strengths of $\sim$ 8 T for one QL and $\sim$ 45 T for five QLs. To predict the behavior at smaller fields, we either use numerical fitting or, when it is appropriate, we interpolate the results of our calculations between $B = 0$ and the smallest field accessible for a given thickness. We employ the Lanczos method of diagonalization at each k point in the magnetic Brillouin zone, and we focus on a small energy window around the Dirac point to reduce the computational load.

As one varies the parameter p/q, a nontrivial fractal pattern in the electronic spectrum, known as the Hofstadter butterfly [21], emerges. First predicted for electrons on a square two-dimensional (2D) lattice, the pattern has been obtained for other 2D lattices (honeycomb [22], triangular [23]), and a generalization to the 3D case has been demonstrated [24]. In this work, we calculate the Hofstadter butterfly for a slab of Bi_2Se_3 with varying thickness. By focusing on the low-field (low-flux) region of the Hofstadter spectrum, which is typically the region probed in experiment, we will show the emergence of well-resolved LLs.

III. NUMERICAL RESULTS

We start with the calculation of LLs in ultrathin films of Bi_2Se_3. Figure 2(a) shows the Hofstadter spectrum of a one-QL-thick slab. Only the results for $\phi/\phi_0 \in [0,1]$ are shown for better visibility. As in the case of a one-band triangular lattice model [23], the spectrum is not symmetric with respect

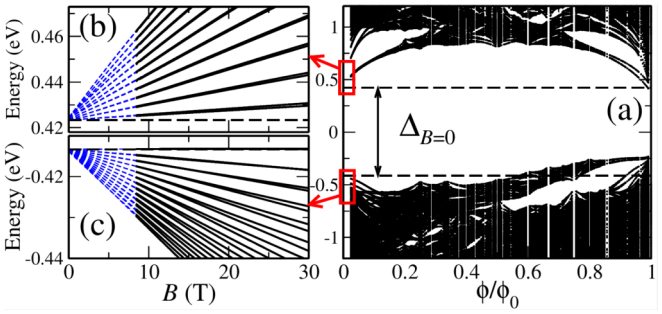

FIG. 2. (Color online) (a) Hofstadter spectrum of one QL of Bi_2Se_3. Positive (b) and negative (c) branches of the LL spectrum (the lowest 24 levels are shown for each branch). Thin dashed lines show the results of numerical fitting for $B < 8.3$ T. Horizontal lines mark the zero-field energy gap.

to $\phi/\phi_0 = 1/2$ since the elementary placket, i.e., the smallest loop in the x-y plane pierced by magnetic flux, is a fraction of the unit cell (Fig. 1). At $B = 0$ there is a large energy gap, $\Delta_{B=0} = 0.84$ eV, due to intersurface hybridization. This gap persists at finite magnetic fields. The field dependence of the gap is quite complex, especially for large values of ϕ/ϕ_0, where the interplay between the periodic lattice potential and the quantizing magnetic field is strong. However, in the regime where the broadening of the LLs is sufficiently weak so that few lowest levels can be resolved ($\phi/\phi_0 \lesssim 0.1$), the gap increases with magnetic field.

We now focus on two regions of the spectrum, marked by red boxes in Fig. 2(a), corresponding to small fields ($B \leqslant 30$ T) and energies around the zero-field gap. There are two distinct branches of the LL spectrum, namely positive and negative [Figs. 2(b) and 2(c), respectively], with well-resolved levels. For the positive branch, the LLs come in pairs, originating from doubly generate states at $B = 0$. The levels disperse almost linearly with magnetic field, in striking similarity with an ordinary 2D electron gas. A similar pattern is found for the negative branch, with the exception of the top LL, which depends weakly on B in this range but starts to deflect downward for $B > 40$ T.

In the same way, we calculate the Hofstadter spectra and the LLs for two to six QLs. The results are summarized in Fig. 3, where we analyze the hybridization gap as a function of magnetic field and slab thickness. Note that for $B = 10$ T we perform numerical interpolations for all thicknesses except one QL. For $B = 45$ T, an interpolation is only required for the largest thickness of six QLs. Figure 3(a) shows that the gap increases with magnetic field for all slabs considered. The dependence is predominantly linear. By using numerical fitting, we determine numerically the linear (dominant) coefficient a_1 in the field dependence, and we plot it versus the thickness in Fig. 3(b). As one can see, the field dependence becomes weaker for thicker slabs. At the same time, the gap decreases exponentially with the thickness, as shown in Fig. 3(c). At $B = 0$ this result is well-established. However, here we explicitly demonstrate the exponential decay at finite fields. As the thickness increases beyond five QLs, the gap becomes exponentially small and field-independent. Hence, in the limit of an infinitely thick slab, the expected LL structure, with a doubly degenerate field-independent $n = 0$ level, is recovered.

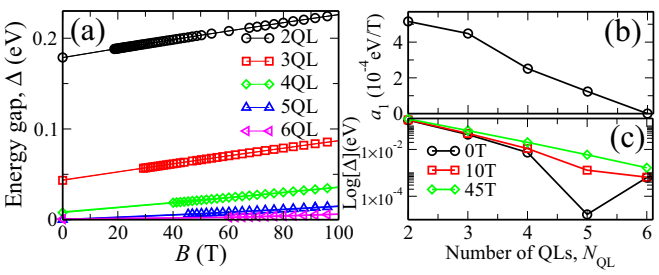

FIG. 3. (Color online) (a) Hybridization gap as a function of magnetic field (including $B = 0$) for two to six QLs of Bi_2Se_3. Symbols show the data points. Solid lines are numerical interpolations in the low-field region. Coefficient of the linear term in the field dependence of the gap (b) and the logarithm of the gap (c) vs thickness for $B = 0$, 10, and 45 T.

The existence of the hybridization gap at finite magnetic fields was investigated in Ref. [8] using the low-energy model of Refs. [17,18]. Within this approach, the particle-hole symmetry is imposed from the start, and therefore the model is unable to capture the asymmetry of the LL spectrum and the strong hybridization with the valence band, which is significant in Bi_2Se_3. Our approach is free from these limitations and provides qualitatively and quantitatively accurate description of these features that are crucial in thin films.

In Ref. [8], the gap was found to depend weakly on magnetic field, oscillating as a function of the thickness, in analogy with the zero-field gap found in other continuum models [18,25,26]. We find that at $B = 0$ the gap exhibits nonmonotonic behavior at certain thicknesses, which resembles the oscillations in these continuum models. The nonmonotonicity is also present at $B \neq 0$, but it is smoothed out at large fields [Fig. 3(c)]. The analytical expression for the gap in Ref. [8] contains a term linear in B (multiplied by an oscillatory and exponentially decaying function of thickness). This is consistent with our calculations but only for moderate field strengths: at large fields the field dependence in our model is highly nonlinear [Fig. 2(a)], in contrast to the result of the continuum model.

The field dependence of LLs that we find in ultrathin films at low magnetic fields (Fig. 2) is clearly distinct from the square-root behavior expected from the Dirac-Hamiltonian description of the surface states. Together with the absence of the $n = 0$ level and a sizable hybridization gap below five QLs (Fig. 3), these results demonstrate that the Dirac fermion picture does not capture the magnetic-field response of 3D TI thin films at moderate magnetic-field strengths.

For typical magnetic-field strengths and disorder strength, the five QL thickness marks a crossover to the range beyond which the topologically protected bulk TI surface state is robustly manifested [17]. This suggests that a nearly degenerate $n = 0$ LL is expected to appear at this thickness at finite magnetic fields. The calculated LL spectrum for 5QLs is shown in Fig. 4(a). We compare our results with the analytical expression for the LLs of the surface states, obtained in Ref. [18], using a low-energy effective Hamiltonian under the assumption of decoupled bulk and surface states.

By setting the Zeeman term to zero in the analytical formula of Liu *et al.* [18], we find that the energy of the $n = 0$ level is given by $E_0 = \tilde{C}_0 + e\tilde{C}_2 B/\hbar$, where $\tilde{C}_{0(1)}$ are the parameters of the model. The term $\propto \tilde{C}_2 B$ can be traced back to the nonlinear (quadratic) term $\tilde{C}_2 k^2$ in the Hamiltonian of the surface states as a function of momentum k, characteristic of the complex electronic structure of the material. Although at low fields the $n = 0$ level is nearly constant, the field dependence becomes significant already at $B \sim 20$ T.

In our calculations at finite fields, two distinct levels with a quasilinear dispersion emerge close to the original Dirac point. We interpret this pair of levels as the two components of $n = 0$ LL, split by intersurface coupling. This splitting is not captured by the effective model of Ref. [18] for the surface states of a semi-infinite system. However, the field dependence of the highest of these two levels matches remarkably well the analytical curve (the position of the Dirac point in the analytical expression has been adjusted to that found in our calculations,

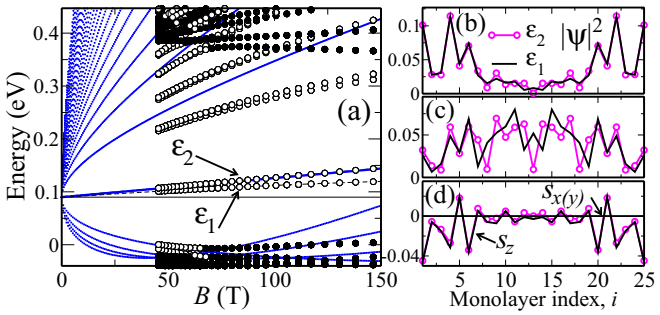

FIG. 4. (Color online) (a) LL spectrum of five QLs of Bi_2Se_3. Open (filled) symbols are for surface (bulk) states. Dashed lines are numerical interpolations for the $n = 0$ level. Solid lines are the analytical surface LLs from Ref. [18]. The horizontal line in (a) marks the position of the Dirac point at $B = 0$. Wave functions $|\psi|^2$ (b,c) and expectation values of the spins $s_{x(y,z)}$ (d) of the two components of the $n = 0$ LL, marked as ε_1 and ε_2 in (a), plotted vs distance along the width of the slab. In (b) and (d), $B = 45$ T; in (c), B is ten times larger.

i.e., ∼0.09 eV). In the limit $B \to 0$, we expect the numerical and analytical results to converge, as confirmed by numerical interpolation (apart from a small but non-negligible gap at zero field). For the higher-index LLs, we find significant deviations from the analytical results. These features are due to the finite thickness of the sample and to higher-order nonlinearities in the electronic structure that are captured by our model.

The two components of the $n = 0$ level are the true surface states, as one can see from the real-space distribution of their wave functions along the slab [Fig. 4(b)]. In fact, their wave functions are almost indistinguishable from the ones calculated at zero field. The surface character is preserved in fields as large as 100 T. The levels have the same spin polarization and are nearly fully spin-polarized in the direction opposite to the magnetic field [Fig. 4(d)]. This finding is consistent with the analytical prediction of Ref. [8]. The splitting between the two $n = 0$ levels increases with magnetic field. For five QLs, we find a splitting of 6 meV at 45 T and we estimate the splitting to be 3 meV at 20 T.

Our calculations capture the strong asymmetry of the LL spectrum with respect to the Dirac point observed in experiments [4,5] and the mixing between bulk and surface states. The asymmetry is mainly due to the fact that the Dirac point is close to the valence band. As a result, the negative branch has only a few well-resolved LLs, which merge with the bulk states with increasing magnetic field. On the contrary, the positive branch contains many levels that preserve their surface character at large fields. Based on the real-space analysis of wave functions, the states roughly in the energy window $[-0.02; 0.4]$ eV are surface states, while the ones outside this window are bulk states. Importantly, the character of the states does not remain constant, and some of the states evolve from surface- to bulklike as the field increases [see Fig. 4(a)].

This behavior is due to the proximity of the bulk and can be understood using the following semiclassical argument. With increasing magnetic field, the radius of the nth Landau orbit in momentum space, expressed as $k_n = \sqrt{2|n|}/l_B$, with $l_B = \sqrt{\hbar/|e|B}$ being the magnetic length [5], increases. Therefore, the LLs start to involve states at k points further away from Γ. In the band structure of a Bi_2Se_3 thin film, at $k \sim k_n$ the energy bands can be quite different from the linearly dispersed Dirac states, especially below the Dirac point, i.e., close to the valence band. Indeed, for five QLs at $k \approx k_n$, with $k_n \approx 0.3$ Å^{-1} for $B \approx 50$ T and $|n| = 1$, the bulk contribution to the energy bands just below the Dirac point becomes dominant [16]. This also explains why at large fields the lower component of the $n = 0$ LL deflects toward the valence band, while the upper one still follows the analytical curve. Since the lower component is energetically closer to the valence band, it is more affected by the valence-band states, and at very large fields its wave function becomes more bulklike [see Fig. 4(c)].

LLs manifest as peaks in the electronic density of states that can be detected in tunneling spectra measured by scanning tunneling spectroscopy (STS) [4,5]. The energy of the $n = 0$ LL indicates the position of the Dirac point within the energy bands. A scaling analysis of LLs can be used to accurately determine the energy dispersion in 3D TIs [5]. The splitting of the $n = 0$ LL studied in this work is detectable by STS at moderate magnetic fields. Hence, it can be used as an alternative sensitive probe of the intersurface hybridization, and in particular of the hybridization gap.

LLs are typically associated with the physics of the quantum Hall effect (QHE). The structure of LLs is embodied in the optical conductivity tensor calculated in the presence of a magnetic field, in the framework of linear-response theory. This yields an estimate of the Hall conductivity in the QHE regime, and it allows, in general, the calculation of magneto-optical effects [27]. We expect the features of the LLs in 3D TI thin films predicted in the present work to affect the structure and position of the Hall plateaus as a function of the chemical potential [9,10].

IV. CONCLUSIONS

In conclusion, we presented a microscopic study of Landau quantization in thin films of Bi_2Se_3. We find that the $n = 0$ level is absent in ultrathin films. For a thin film containing five QLs, the degeneracy of the $n = 0$ level is lifted due to hybridization between top and bottom surface states, with the two components being strongly spin-polarized. Since it is now possible to probe the properties of 3D TIs in strong magnetic fields ($\gtrsim 20$ T) [28] and to measure sub-meV gaps in thin films of 3D TIs [29], these spin-polarized states with a splitting of a few meV can be measured experimentally. The nontrivial structure of Landau levels, originating from the realistic band structure and the intersurface coupling, will affect the properties of 3D TI thin films in magnetic field, in particular magneto-optical properties, the surface quantum Hall effect, and the quantum anomalous Hall effect.

ACKNOWLEDGMENTS

This work was supported by the Faculty of Natural Sciences at Linnaeus University and by the Swedish Research Council under Grant No. 621-2010-3761. A.H.M. was supported by the Welch Foundation under Grant No. TBF1473 and by the

DOE Division of Materials Sciences and Engineering under Grant No. DE-FG03-02ER45958. Computational resources have been provided by the Lunarc Center for Scientific and Technical Computing at Lund University.

[1] M. Z. Hasan and C. L. Kane, Rev. Mod. Phys. **82**, 3045 (2010).
[2] X.-L. Qi and S.-C. Zhang, Rev. Mod. Phys. **83**, 1057 (2011).
[3] D. Hsieh, Y. Xia, D. Qian, L. Wray, J. H. Dil, F. Meier, J. Osterwalder, L. Patthey, J. G. Checkelsky, N. P. Ong, A. V. Fedorov, H. Lin, A. Bansil, D. Grauer, Y. S. Hor, R. J. Cava, and M. Z. Hasan, Nature (London) **460**, 1101 (2009).
[4] P. Cheng, C. Song, T. Zhang, Y. Zhang, Y. Wang, J.-F. Jia, J. Wang, Y. Wang, B.-F. Zhu, X. Chen, X. Ma, K. He, L. Wang, X. Dai, Z. Fang, X. Xie, X.-L. Qi, C.-X. Liu, S.-C. Zhang, and Q.-K. Xue, Phys. Rev. Lett. **105**, 076801 (2010).
[5] T. Hanaguri, K. Igarashi, M. Kawamura, H. Takagi, and T. Sasagawa, Phys. Rev. B **82**, 081305 (2010).
[6] Y. Okada, W. Zhou, C. Dhital, D. Walkup, Y. Ran, Z. Wang, S. D. Wilson, and V. Madhavan, Phys. Rev. Lett. **109**, 166407 (2012).
[7] J. Martin, N. Akerman, G. Ulbricht, T. Lohmann, K. von Klitzing, J. H. Smet, and A. Yacoby, Nat. Phys. **5**, 669 (2009).
[8] Z. Yang and J. H. Han, Phys. Rev. B **83**, 045415 (2011).
[9] A. A. Zyuzin and A. A. Burkov, Phys. Rev. B **83**, 195413 (2011).
[10] M. Tahir, K. Sabeeh, and U. Schwingenschlögl, J. Appl. Phys. **113**, 043720 (2013).
[11] Y. Jiang, Y. Wang, M. Chen, Z. Li, C. Song, K. He, L. Wang, X. Chen, X. Ma, and Q.-K. Xue, Phys. Rev. Lett. **108**, 016401 (2012).
[12] E. Brown, Phys. Rev. **133**, A1038 (1964).
[13] F. A. Butler and E. Brown, Phys. Rev. **166**, 630 (1968).
[14] M. Graf and P. Vogl, Phys. Rev. B **51**, 4940 (1995).
[15] K. Kobayashi, Phys. Rev. B **84**, 205424 (2011).
[16] A. Pertsova and C. M. Canali, New J. Phys. **16**, 063022 (2014).
[17] Y. Zhang, K. He, C.-Z. Chang, C.-L. Song, L.-L. Wang, J.-F. Chen, X. Jia, Z. Fang, X. Dai, W.-Y. Shan, S.-Q. Shen, Q. Niu, X.-L. Qi, S.-C. Zhang, X.-C. Ma, and Q.-K. Xue, Nat. Phys. **6**, 584 (2010).
[18] C.-X. Liu, X.-L. Qi, H.-J. Zhang, X. Dai, Z. Fang, and S.-C. Zhang, Phys. Rev. B **82**, 045122 (2010).
[19] H.-J. Zhang, C.-X. Liu, X.-L. Qi, X.-Y. Deng, X. Dai, S.-C. Zhang, and Z. Fang, Phys. Rev. B **80**, 085307 (2009).
[20] R. Peierls, Z. Phys **80**, 763 (1933).
[21] D. R. Hofstadter, Phys. Rev. B **14**, 2239 (1976).
[22] R. Ramal, J. Phys. (Paris) **46**, 1345 (1985).
[23] G.-Y. Oh, Phys. Rev. B **63**, 087301 (2001).
[24] M. Koshino, H. Aoki, K. Kuroki, S. Kagoshima, and T. Osada, Phys. Rev. Lett. **86**, 1062 (2001).
[25] J. Linder, T. Yokoyama, and A. Sudbø, Phys. Rev. B **80**, 205401 (2009).
[26] H.-Z. Lu, W.-Y. Shan, W. Yao, Q. Niu, and S.-Q. Shen, Phys. Rev. B **81**, 115407 (2010).
[27] W.-K. Tse and A. H. MacDonald, Phys. Rev. B **84**, 205327 (2011).
[28] J. G. Analytis, R. D. McDonald, S. C. Riggs, J. H. Chu, G. S. Boebinger, and I. R. Fisher, Nat. Phys. **6**, 960 (2010).
[29] D. Kim, P. Syers, N. P. Butch, J. Paglione, and M. S. Fuhrer, Nat. Commun. **4**, 2040 (2013).